Chemical
Science

ROYAL SOCIETY
OF CHEMISTRY

EDGE ARTICLE

View Article Online
View Journal | View Issue

Check for updates

Cite this: *Chem. Sci.*, 2023, **14**, 10795

All publication charges for this article have been paid for by the Royal Society of Chemistry

Received 24th May 2023
Accepted 19th September 2023

DOI: 10.1039/d3sc02604c

rsc.li/chemical-science

Rare-earth hydroxide/MXene hybrid: a promising agent for near-infrared photothermy and magnetic resonance imaging†

Mingjun Bai,[abc] Linawati Sutrisno,[de] Junhong Duan,[f] Hao Wan,*[b] Gen Chen,[g] Xiaohe Liu*[bg] and Renzhi Ma*[c]

Layered gadolinium hydroxide (LGdH) and Ti_3C_2 monolayers were assembled into a LGdH/Ti_3C_2 (GTC) hybrid. The hybrid demonstrated enhanced near-infrared (NIR) light absorption properties and superior photothermal performance. Moreover, the GTC hybrid achieved an excellent T1-weighted magnetic resonance imaging (MRI) effect.

Introduction

Titanium carbide (Ti_3C_2), the first reported MXene, is synthesized by selective etching of the parent MAX phase of layered Ti_3AlC_2, which has attracted tremendous attention for various applications including energy storage and conversion, drug delivery and environmental remediation.[1–6] Recent reports show that MXenes with excellent biocompatibility and low toxicity are promising materials in biochemistry fields, such as immunomodulation and tissue reconstruction,[7,8] 3D bioprinting,[9,10] bioimaging,[11] biosensing,[11] and photothermal therapy.[12–14] The etching process involves the surface modification of MXenes with functional groups –OH, –F, =O, or –$Al(OH)_4$, resulting in enhanced photothermal properties.[15,16] But the photothermal performance of Ti_3C_2 in the NIR window is still limited and further improvement is required.[17,18] Therefore, it is of great significance to modify Ti_3C_2 MXene with other functional materials, such as 2D nanosheets,[19,20] to elevate its photothermal performance as well as expand its multi-functionality.

Layered rare-earth hydroxides (LREHs), a new important family of anion-exchangeable layered compounds, show promising applications in the fields of magnetism[21–23] and photoluminescence[24,25] due to special 4f electronic structures. In recent years, more and more research interest has been invested in exploring the biochemical applications of rare earth-containing materials.[26–28] However, biochemical research is mainly focused on rare-earth element-doped nanomaterials or quantum dots.[27,29,30] Exploration and hybridization of 2D LREHs with other nanosheets are still blank. Recently, the successful exfoliation of LREHs into monolayer nanosheets has greatly expanded their application prospects as building blocks in nanofilms and nanodevices.[31,32] For example, through layer-by-layer assembly, superlattice structured films constructed from LREH nanosheets and semiconducting oxide nanosheets exhibited enhanced photoluminescence through efficient energy transfer across the nanointerface.[32,33] Among rare-earth elements, gadolinium and gadolinium-based compounds are widely used as photoluminescent hosts or matrices due to low phonon energy, suitability for coupling with other rare-earth ions, and low cost. Moreover, gadolinium compounds with the half-filled 4f orbitals of Gd^{3+}, exhibit excellent magnetism properties making them ideal for use as magnetic resonance imaging (MRI) and computed tomography (CT) contrast agents.[34–37] Therefore, a layered gadolinium hydroxide (LGdH) nanosheet is selected to pair with a Ti_3C_2 nanosheet for enhanced photothermal and MRI properties.

In this work, unilaminar LGdH and Ti_3C_2 nanosheets were face-to-face restacked into a LGdH/Ti_3C_2 (GTC) hybrid, which exhibited enhanced NIR light absorption and MRI performance. This approach not only broadens the application of both MXenes and LREHs nanosheets toward biotherapy, but also provides a general strategy to design photothermal therapy and MRI contrast agent materials based on 2D nanomaterials.

---

[a] *College of Materials Science and Engineering, Chongqing University of Technology, Chongqing 400054, P. R. China*

[b] *Zhongyuan Critical Metals Laboratory, Zhengzhou University, Zhengzhou 450001, P. R. China. E-mail: wanhao@zzu.edu.cn; liuxh@csu.edu.cn*

[c] *Research Center for Materials Nanoarchitectonics (MANA), National Institute for Materials Science (NIMS), Tsukuba, Ibaraki 305-0044, Japan. E-mail: MA.Renzhi@nims.go.jp*

[d] *Department of Materials Science and Engineering, Graduate School of Pure and Applied Sciences, Tsukuba, Ibaraki 305-8577, Japan*

[e] *Research Center for Functional Materials, National Institute for Materials Science (NIMS), Tsukuba, Ibaraki 305-0044, Japan*

[f] *Department of Radiology, The Third Xiangya Hospital, Central South University, Changsha, Hunan 410013, P. R. China*

[g] *School of Materials Science and Engineering, Central South University, Changsha, Hunan 410083, P. R. China*

† Electronic supplementary information (ESI) available. See DOI: **https://doi.org/10.1039/d3sc02604c**

Results and discussion

Scanning electron microscopy (SEM) images of Ti_3AlC_2 before and after etching are shown in Fig. S1a and b.† Raw Ti_3AlC_2 swelled and split obviously after etching. According to inductively coupled plasma-optical emission spectrometry (ICP-OES) analysis, the Al/Ti atomic ratio was estimated to be 0.007 : 3 after etching, verifying an almost complete removal of the Al atoms. Fig. S1c† shows the X-ray diffraction (XRD) profile of the raw Ti_3AlC_2 particles. The pattern matched well with the standard JCPDS card of the hexagonal Ti_3AlC_2 phase (No. 52-0875), indicating a high crystallinity and phase purity of the pristine crystals. After etching, the *00l* peaks slightly shifted to a lower degree, corresponding to an expanded interlayer distance from 1.84 nm to 2.05 nm. In addition, the broader full width at half maximum (FWHM) implied a decreased layer stacking order.

Fig. 1a and b show the atomic force microscopy (AFM) image and thickness profile of exfoliated Ti_3C_2 nanosheets, respectively. They were characterized by a typical thickness of approximately 1.5 nm, which is larger than a crystallographic unilamellar thickness of 0.75 nm,[16] likely due to the adsorption of functional groups/ions (such as –OH and –F) and water molecules on the surface. Similarly, Fig. 1c and d show the AFM image and typical thickness of LGdH nanosheets, separately. The thickness was estimated to be approximately 1.0 nm, which is consistent with our previous report,[31] indicating a monolayer feature. The lateral dimensions of both nanosheets fall in a range from several hundred nanometres to a few micrometres. The inset photographs of the suspensions in Fig. 1a and c display a homogeneous and stable dispersion state of the exfoliated nanosheets.

A black flocculated product was induced immediately with the dropwise addition of Ti_3C_2 nanosheets into the LGdH nanosheet suspension. As the Ti_3C_2 nanosheets held a negative charge with a zeta potential of −34.6 mV while their LGdH counterparts were positively charged with a zeta potential of +57.3 mV, they underwent spontaneous restacking driven by the electrostatic attraction (see Fig. S2† for details). Fig. S3a† depicts the XRD pattern of the flocculated product GTC. Both the characteristic in-plane diffraction peaks of LGdH and Ti_3C_2 were observed, confirming the intact feature of two oppositely charged nanosheets during the hybridizing process. Fig. 2a shows the transmission electron microscopy (TEM) image of the resultant GTC hybrid, in which lamellar morphology was observed. The rings in the selected area electron diffraction (SAED) pattern are indexed to be in-plane reflections of Ti_3C_2 nanosheets and LGdH nanosheets, respectively (Fig. 2b). The elemental mapping in Fig. 2c indicates a uniform distribution and intimate mixing of the two nanosheets in the GTC hybrid. The size of the GTC hybrid ranged from 50 to 500 nm according to the dynamic light scattering (DLS) results in Fig. S3b.† The

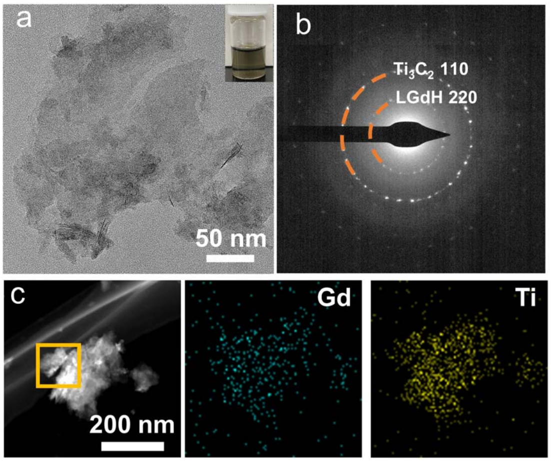

Fig. 2 (a) TEM, (b) SAED pattern, and (c) elemental mapping images of the GTC hybrid. The inset of (a) shows the corresponding suspension.

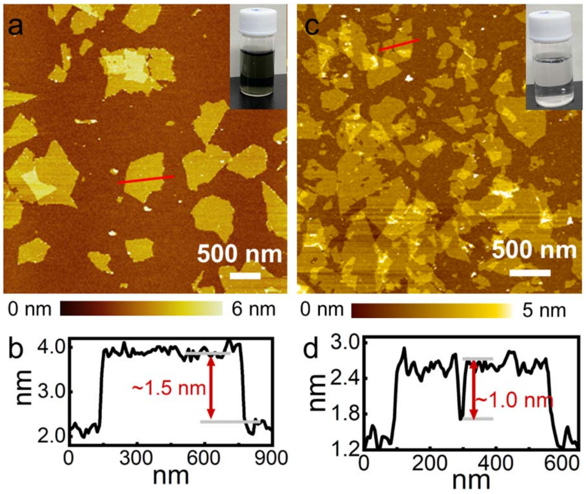

Fig. 1 AFM images of (a) Ti_3C_2 and (c) LGdH nanosheets. Corresponding height profiles of (b) Ti_3C_2 and (d) LGdH nanosheets along the marked lines. Insets of (a) and (c) show the photographs of the nanosheet suspension.

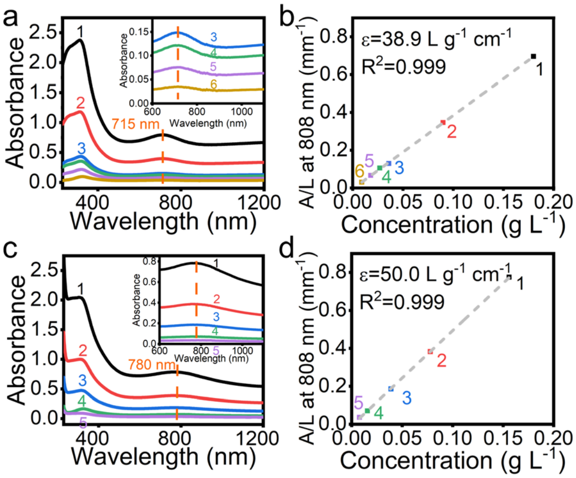

Fig. 3 UV-vis absorption of (a) Ti_3C_2 nanosheet suspensions and (c) GTC hybrid suspensions. The Lambert–Beer law absorbance plot for absorption at 808 nm of (b) Ti_3C_2 nanosheet suspensions and (d) GTC hybrid suspensions. The numbers 1–6 stand for different concentrations of each suspension.

smaller size of the flocculated GTC is due to the bending and wrinkles of the nanosheets during the flocculation process. It is noteworthy that flocculated GTC hybrid can be well re-dispersed in deionized water, as evidenced by the inset of Fig. 2a. The small size and uniform dispersion features of the flocculated product made it possible to be used in biomedicine fields such as MRI and photothermal therapy.

Fig. 3 compares UV-vis absorbance of Ti_3C_2 nanosheets and the GTC hybrid at various concentrations. For the convenience of comparison, all the concentrations were calibrated using the quantity of Ti_3C_2 in the suspensions. The concentrations of all samples in Fig. 3 are tabulated in Table S1.† As shown in Fig. 3a, for pure Ti_3C_2 nanosheet suspensions, the strong and broad absorption band ranging from 230 to 500 nm was attributed to the band-gap energy of the oxidized MXene.[38] In addition, the weak broad absorption band centred at 715 nm in the NIR range from 600 to 830 nm was due to the surface plasmon resonance (SPR) caused by the inter-band transitions in MXene nanosheets.[39] As an important parameter to evaluate the efficiency of light absorption, the mass extinction coefficient ε at 808 nm can be calculated according to the Lambert–Beer law:

$$A = \varepsilon c l$$

where A is the absorbance, ε represents the absorption coefficient, c (g L^{-1}) stands for the concentration of the samples and l (cm) is the absorption path length. Based on the plot shown in Fig. 3b, the ε of Ti_3C_2 nanosheets was calculated to be 38.9 L g^{-1} cm^{-1}. This value was higher than those reported in the previous literature (Table S2†).[16,40] In the current work, the Al atomic layer in the Ti_3AlC_2 parent compound was selectively etched using LiF/HCl solvent. Some residual Li^+ ions adsorbed on the surface of the Ti_3C_2 nanosheets,[41] which was confirmed by the ICP result yielding a molar ratio of Ti : Al : Li at 94.28 : 0.23 : 5.49. Similar to Al or Au ion modified Ti_3C_2 MXene, the adsorption of Li^+ ions may enhance the local surface plasmon resonance (LSPR) effect,[18,40] resulting in an enhancement in NIR light absorption properties. As shown in Fig. 3c, for the GTC hybrid, the broad band in the NIR region red-shifted to 780 nm and the absorption was extended to a wider wavelength range from 600 to 1000 nm. Compared to 38.9 L g^{-1} cm^{-1} for Ti_3C_2 nanosheets, the ε value of the GTC hybrid increased to 50.0 L g^{-1} cm^{-1}, the highest value among those of the reported NIR photothermal materials (Table S2†). In contrast, the same amount of pure LGdH nanosheets showed negligible absorption in the NIR region (Fig. S4†). The red-shift absorption and enhanced mass extinction coefficient of the GTC hybrid are believed to be a synergistic effect of hybridizing LGdH and Ti_3C_2 nanosheets on a molecular scale. The outstanding NIR absorption properties of the GTC hybrid promise their high photothermal performance.

The photothermal properties were evaluated under NIR laser exposure with a laser intensity of 2 W cm^{-2}. The concentration of a pure Ti_3C_2 suspension and LGdH suspension was 15.6 mg mL^{-1}. While for the GTC suspension, the contained Ti_3C_2 component was 15.6 mg mL^{-1}. As indicated by the IR thermographic images in Fig. S5,† the temperature of the GTC hybrid increased with an increasing concentration. Under 2 W cm^{-2} irradiation for 10 min, the temperature surpassed 60.4 °C when

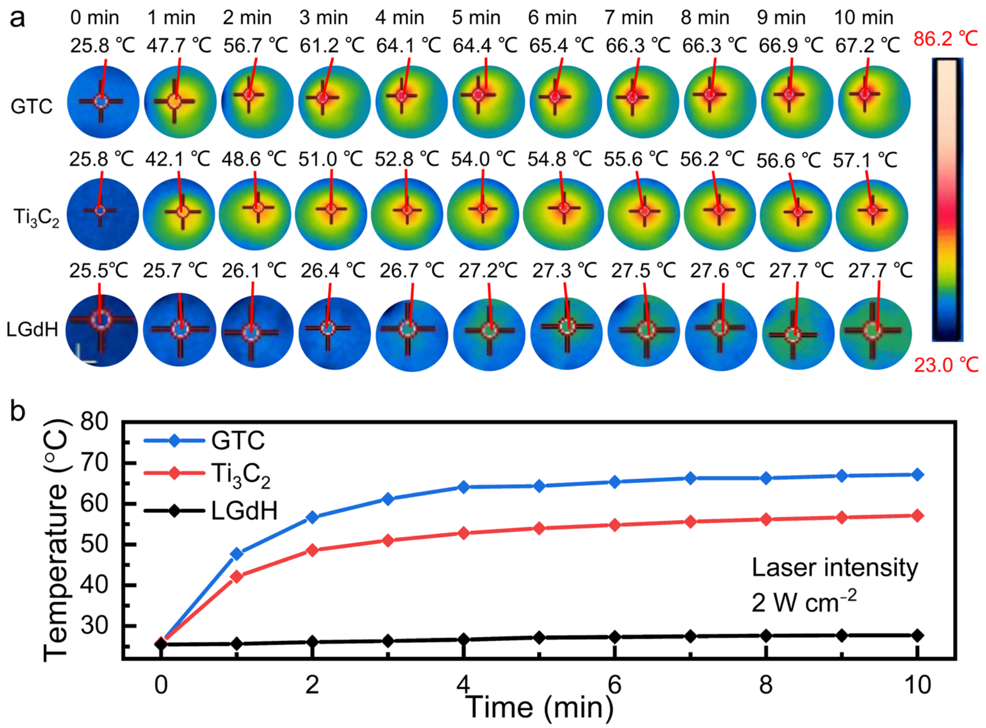

Fig. 4 Photothermal properties. (a) IR thermographic images and (b) heating curves of the GTC hybrid, Ti_3C_2 nanosheets and LGdH nanosheets at a calibrated concentration of Ti_3C_2 of 15.6 mg mL^{-1} under NIR laser irradiation (808 nm, 2 W cm^{-2}).

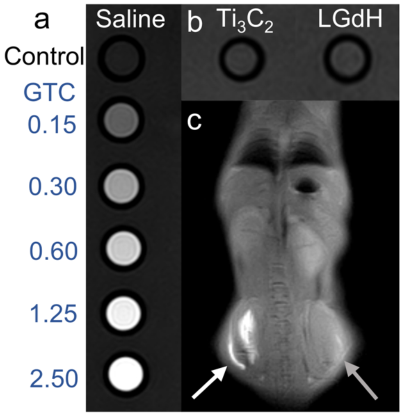

Fig. 5 *In vitro* T1-weighted MRI effect of (a) the GTC hybrid at various concentrations (mg mL^{-1}), and (b) individual Ti_3C_2 nanosheet and LGdH nanosheet suspensions at a concentration of 1.25 mg mL^{-1}. (c) *In vivo* MRI of a nude mouse with injection of the GTC suspension (white arrow) and the control saline (grey arrow).

the concentration was higher than 7.8 mg mL^{-1}. For instance, for an elevated concentration of 15.6 mg mL^{-1}, the temperature of GTC drastically rose to 61.2 °C after a short exposure of only 3 min, and finally reached 67.2 °C after 10 min. In comparison, the temperature reached only 57.1 °C and 27.7 °C for pure Ti_3C_2 and LGdH nanosheets, respectively, as presented in Fig. 4. The result was well consistent with that of the UV-vis absorption analysis, in which the ε value of the GTC hybrid was notably higher than that of Ti_3C_2 nanosheets, while the LGdH nanosheet exhibited negligible NIR absorption. The significant temperature growth induced by the GTC hybrid indicated a higher photothermal capability than that by using sole Ti_3C_2 or LGdH nanosheets.

The performance of the GTC hybrid as a T1-weighted MRI contrast agent was evaluated by an *in vitro* assay experiment. As shown in Fig. 5a and b, the contrast effect was enhanced with the increasing concentration of the GTC hybrid, while no significant enhancement for individual Ti_3C_2 nanosheet and LGdH nanosheet suspensions was observed when compared with the control saline group. When the concentration reached 1.25 mg mL^{-1}, the T1-weighted signal exhibited obvious brightness compared with that of the control group, comparable to the frontier contrast agents such as clinical gadoteric acid meglumine salt injection.[42] Fig. 5c depicts the *in vivo* contrast effect of both the GTC suspension (white arrow) and the control saline (grey arrow), from which a T1-weighted signal image was clearly presented. The significant enhancement in both *in vitro* and *in vivo* tests implied a promising application of the GTC hybrid as an MRI agent.

Conclusions

In conclusion, a GTC hybrid was fabricated by the assembly of oppositely charged Ti_3C_2 nanosheets and their LGdH counterparts. The hybrid showed a significantly improved mass absorption coefficient ε of 50.0 L g^{-1} cm^{-1} at 808 nm compared with 38.9 L g^{-1} cm^{-1} for Ti_3C_2 nanosheets. Under NIR laser (808 nm, 2 W cm^{-2}) irradiation for 10 min, the temperature of the GTC hybrid could reach as high as 67.2 °C, demonstrating a higher photothermal capability than sole Ti_3C_2 and LGdH nanosheets. Moreover, the GTC hybrid showed an excellent T1-weighted MRI effect. This work may hold great potential for the design and development of high-performance photothermal therapy materials as well as MRI contrast agents through the molecular-level hybridization of fancy nanosheet building blocks.

Author contributions

M. B. and R. M. conceived and coordinated the project. X. L., H. W. and R. M. supervised the project. M. B. performed the experiments and analysed the data. L. S. assisted with the photothermal property measurement and analysis. J. D. assisted with the MRI measurement and data analysis. The manuscript was written through the contributions of all authors. All authors have given approval to the final version of the manuscript.

Conflicts of interest

The authors declare no competing financial interest.

Acknowledgements

The authors acknowledge the financial support from the National Natural Science Foundation of China (U20A20123) and the Innovative Research Group of the Hunan Provincial Natural Science Foundation of China (2019JJ10006). M. B. is thankful for the support from the Chongqing University of Technology (2023ZDZ026) and the Science and Technology Research Program of the Chongqing Municipal Education Commission (KJQN202301134). R. M. acknowledges the support from JSPS KAKENNHI (22H01916 and 22K18956). Prof. Guoping Chen from the National Institute for Materials Science, Tsukuba, Japan is gratefully acknowledged.

Notes and references

1 M. Naguib, M. Kurtoglu, V. Presser, J. Lu, J. Niu, M. Heon, L. Hultman, Y. Gogotsi and M. W. Barsoum, *Adv. Mater.*, 2011, **23**, 4248–4253.
2 A. Levitt, J. Zhang, G. Dion, Y. Gogotsi and J. M. Razal, *Adv. Funct. Mater.*, 2020, **30**, 2000739.
3 L. Yu, Z. Fan, Y. Shao, Z. Tian, J. Sun and Z. Liu, *Adv. Energy Mater.*, 2019, **9**, 1901839.
4 Q. Liu, A. Zhao, X. He, Q. Li, J. Sun, Z. Lei and Z. H. Liu, *Adv. Funct. Mater.*, 2021, **31**, 2010944.
5 J. Lei, F. Yu, H. Xie and J. Ma, *Chem. Sci.*, 2023, **14**, 3610–3621.
6 A. E. Allah, J. Wang, Y. V. Kaneti, T. Li, A. A. Farghali, M. H. Khedr, A. K. Nanjundan, B. Ding, H. Dou and X. Zhang, *Nano Energy*, 2019, **65**, 103991.
7 S. Pan, J. Yin, L. Yu, C. Zhang, Y. Zhu, Y. Gao and Y. Chen, *Adv. Sci.*, 2020, **7**, 1901511.

8 A. Rafieerad, W. Yan, G. L. Sequiera, N. Sareen, E. Abu-El-Rub, M. Moudgil and S. Dhingra, *Adv. Healthcare Mater.*, 2019, **8**, 1900569.

9 H. Rastin, B. Zhang, A. Mazinani, K. Hassan, J. Bi, T. T. Tung and D. Losic, *Nanoscale*, 2020, **12**, 16069–16080.

10 M. Das, R. S. Ambekar, S. K. Panda, S. Chakraborty and C. S. Tiwary, *J. Mater. Res.*, 2021, **36**, 4024–4050.

11 M. Soleymaniha, M. A. Shahbazi, A. R. Rafieerad, A. Maleki and A. Amiri, *Adv. Healthcare Mater.*, 2019, **8**, 1801137.

12 H. Lin, X. Wang, L. Yu, Y. Chen and J. Shi, *Nano Lett.*, 2017, **17**, 384–391.

13 R. Liang, Y. Li, M. Huo, H. Lin and Y. Chen, *ACS Appl. Mater. Interfaces*, 2019, **11**, 42917–42931.

14 X. Fan, Y. Ding, Y. Liu, J. Liang and Y. Chen, *ACS Nano*, 2019, **13**, 8124–8134.

15 G. Li, B. C. Wyatt, F. Song, C. Yu, Z. Wu, X. Xie, B. Anasori and N. Zhang, *Adv. Funct. Mater.*, 2021, **21**, 2105043.

16 J. Xuan, Z. Wang, Y. Chen, D. Liang, L. Cheng, X. Yang, Z. Liu, R. Ma, T. Sasaki and F. Geng, *Angew. Chem., Int. Ed.*, 2016, **55**, 14569–14574.

17 D. Xu, Z. Li, L. Li and J. Wang, *Adv. Funct. Mater.*, 2020, **30**, 2000712.

18 Z. Yu, L. Jiang, R. Liu, W. Zhao, Z. Yang, J. Zhang and S. Jin, *Chem. Eng. J.*, 2021, **426**, 131914.

19 M. Eguchi, A. S. Nugraha, A. E. Rowan, J. Shapter and Y. Yamauchi, *Adv. Sci.*, 2021, **8**, 2100539.

20 W. Liu, Z. Wang, Y. Su, Q. Li, Z. Zhao and F. Geng, *Adv. Energy Mater.*, 2017, **7**, 1602834.

21 Z. Yang, H. Zhang, M. Bai, W. Li, S. Huang, S. Ruan and Y. J. Zeng, *J. Mater. Chem. C*, 2020, **8**, 11866–11873.

22 L. Caretta, E. Rosenberg, F. Büttner, T. Fakhrul, P. Gargiani, M. Valvidares, Z. Chen, P. Reddy, D. A. Muller, C. A. Ross and G. S. D. Beach, *Nat. Commun.*, 2020, **11**, 1090.

23 H. Wang, J. Chen, T. Liu, J. Zhang, K. Baumgaertl, C. Guo, Y. Li, C. Liu, P. Che, S. Tu, S. Liu, P. Gao, X. Han, D. Yu, M. Wu, D. Grundler and H. Yu, *Phys. Rev. Lett.*, 2020, **124**, 027203.

24 Y. Liu, X. Rong, M. Li, M. S. Molokeev, J. Zhao and Z. Xia, *Angew. Chem., Int. Ed.*, 2020, **59**, 11634–11640.

25 Z. Zeng, Y. Xu, Z. Zhang, Z. Gao, M. Luo, Z. Yin, C. Zhang, J. Xu, B. Huang and F. Luo, *Chem. Soc. Rev.*, 2020, **49**, 1109–1143.

26 Z. Liu, F. Ren, H. Zhang, Q. Yuan, Z. Jiang, H. Liu, Q. Sun and Z. Li, *Biomaterials*, 2019, **219**, 119364.

27 L. Ruiyi, L. Zaijun, S. Xiulan, J. Jan, L. Lin, G. Zhiguo and W. Guangli, *Chem. Eng. J.*, 2020, **382**, 122992.

28 X. Shan, Q. Chen, X. Yin, C. Jiang, T. Li, S. Wei, X. Zhang, G. Sun, J. Liu and L. Lu, *J. Mater. Chem. B*, 2020, **8**, 426–437.

29 D.-K. Ji, G. Reina, H. Liang, D. Zhang, S. Guo, B. Ballesteros, C. Ménard-Moyon, J. Li and A. Bianco, *ACS Appl. Nano Mater.*, 2021, **4**, 1467–1477.

30 H. Li, R. Wei, G.-H. Yan, J. Sun, C. Li, H. Wang, L. Shi, J. A. Capobianco and L. Sun, *ACS Appl. Mater. Interfaces*, 2018, **10**, 4910–4920.

31 M. Bai, X. Liu, N. Sakai, Y. Ebina, L. Jia, D. Tang, T. Sasaki and R. Ma, *J. Phys. Chem. Lett.*, 2021, **12**, 10135–10143.

32 M. Bai, X. Liu, T. Sasaki and R. Ma, *Nanoscale*, 2021, **13**, 4551–4561.

33 S. Ida, Y. Sonoda, K. Ikeue and Y. Matsumoto, *Chem. Commun.*, 2010, **46**, 877–879.

34 X. Yu, X. Liu, W. Wu, K. Yang, R. Mao, F. Ahmad, X. Chen and W. Li, *Angew. Chem., Int. Ed.*, 2019, **58**, 2017–2022.

35 N. Rammohan, K. W. MacRenaris, L. K. Moore, G. Parigi, D. J. Mastarone, L. M. Manus, L. M. Lilley, A. T. Preslar, E. A. Waters, A. Filicko, C. Luchinat, D. Ho and T. J. Meade, *Nano Lett.*, 2016, **16**, 7551–7564.

36 L. M. Manus, D. J. Mastarone, E. A. Waters, X. Q. Zhang, E. A. Schultz Sikma, K. W. MacRenaris, D. Ho and T. J. Meade, *Nano Lett.*, 2010, **10**, 484–489.

37 H. Wan, L. Hu, X. Liu, Y. Zhang, G. Chen, N. Zhang and R. Ma, *Chem. Sci.*, 2023, **14**, 2776–2798.

38 E. Satheeshkumar, T. Makaryan, A. Melikyan, H. Minassian, Y. Gogotsi and M. Yoshimura, *Sci. Rep.*, 2016, **6**, 32049.

39 S. Elumalai, J. R. Lombardi and M. Yoshimura, *Adv. Mater.*, 2020, **1**, 146–152.

40 G. Liu, J. Zou, Q. Tang, X. Yang, Y. Zhang, Q. Zhang, W. Huang, P. Chen, J. Shao and X. Dong, *ACS Appl. Mater. Interfaces*, 2017, **9**, 40077–40086.

41 F. Liu, A. Zhou, J. Chen, J. Jia, W. Zhou, L. Wang and Q. Hu, *Appl. Surf. Sci.*, 2017, **416**, 781–789.

42 J. Li, J. Duan, Z. He, Y. Liao, X. Liu, P. Rong, G. Chen, H. Wan, Y. Huang and R. Ma, *Adv. Opt. Mater.*, 2023, **11**, 2203146.